ELSEVIER

Polymer 42 (2001) 2045–2059

polymer

www.elsevier.nl/locate/polymer

Modeling of a two-stage draw process

S.E. Bechtel[a,*], S. Vohra[a], K.I. Jacob[b]

[a]*Department of Mechanical Engineering, Ohio State University, Columbus, OH 43210, USA*
[b]*School of Textile and Fiber Engineering, Georgia Institute of Technology, Atlanta, GA 30332, USA*

Received 4 February 2000; received in revised form 16 June 2000; accepted 16 June 2000

Abstract

In our earlier work (S.E. Bechtel et al., J Appl Mech 2000;67(1):197–206) we created a model for slip of linearly elastic belts on pulleys, and adapted our model to isothermal draw of fibers on rollers (submitted for publication). Here, we: (i) incorporate temperature dependence, (ii) extend the constitutive characterization to piecewise linearly elastic–plastic fibers to capture the softening behavior of as-spun fibers, and (iii) assemble governing equations for fibers on rollers and in freespans, together with matching conditions, to produce a comprehensive model for a two-stage, non-isothermal industrial draw process. The model is then employed to simulate three representative drawlines.

Keywords: Fiber drawing; Multi-stage draw processes; Non-isothermal draw

1. Introduction

The manufacturing process of a polymer fiber consists of first spinning molten polymer into filaments through a capillary and then uniaxially drawing the solidified filaments. This process of spinning followed by drawing is designed to produce a filament with a desired strength, accomplished by inducing sufficient orientation of the polymer molecules along the axial direction of the filament.

During the spinning process the polymer exits the capillary of the spinneret with a die swell, which removes any molecular orientation in the polymer jet. This isotropic polymeric melt is then stretched in the spinline downstream of the die swell while it cools, inducing orientation of the molecules prior to solidification of the fiber. The relaxation time of the polymer melt is typically comparable to the time available for the fiber before it solidifies, however, thereby undoing much of this orientation, and hence the amount of orientation that can be induced in the fiber during spinning is insufficient to produce the desired strength.

The orientation of the polymer molecules can be increased after the spinning process by a subsequent drawing process, in which the solidified, as-spun fiber is heated to a temperature above the glass transition and drawn with a series of rollers. The purpose of the draw process is to convert relatively weak as-spun fibers to fibers with greater molecular orientation and the resulting greater strength. Draw enhanced morphology and micro-structure is responsible for improved properties of fibers and films [1–6]. Using Nuclear Magnetic Resonance (NMR), Botev et al. [1] show that for polyamide-6 fibers, temperature plays a key role in determining whether the draw is effective. Cansfield et al. [2] studied the effect of windup speeds and draw ratios on the mechanical properties, molecular orientation, and shrinkage behavior of PET fibers. They report that the effect of increasing the windup speed of the spun fiber is similar to an increase in molecular weight and hence the viscosity of the polymer. Postema and Pennings [3] found that homogeneous drawing, achieved by drawing at low deformation rate, is most efficient in improving strength for poly(L-lactide) fibers. Inhomogeneous drawing under high deformation rates with temperature gradients resulted in reduced fiber properties. However, in a manufacturing process it is important to use a draw process with high deformation rate in order to improve productivity. It remains to find the temperature strain rate combinations that optimize fiber properties.

New crystals are formed and redistribution of existing crystals occurs during draw. Salem [4] investigated the influence of uniaxial draw strain on crystallization in PET films, under both constant extension rate and constant strain rate conditions. It was found that at high strain rates the crystallization rate increases, while the pattern gradually reverses as strain rate is reduced. Hermanutz et al. [5] studied the effect of draw, and the resulting micro-structure,

* Corresponding author. Tel.: +1-614-292-6570; fax: +1-614-292-3163.
E-mail address: bechtel.3@osu.edu (S.E. Bechtel).

0032-3861/01/$ - see front matter
PII: S0032-3861(00)00535-8

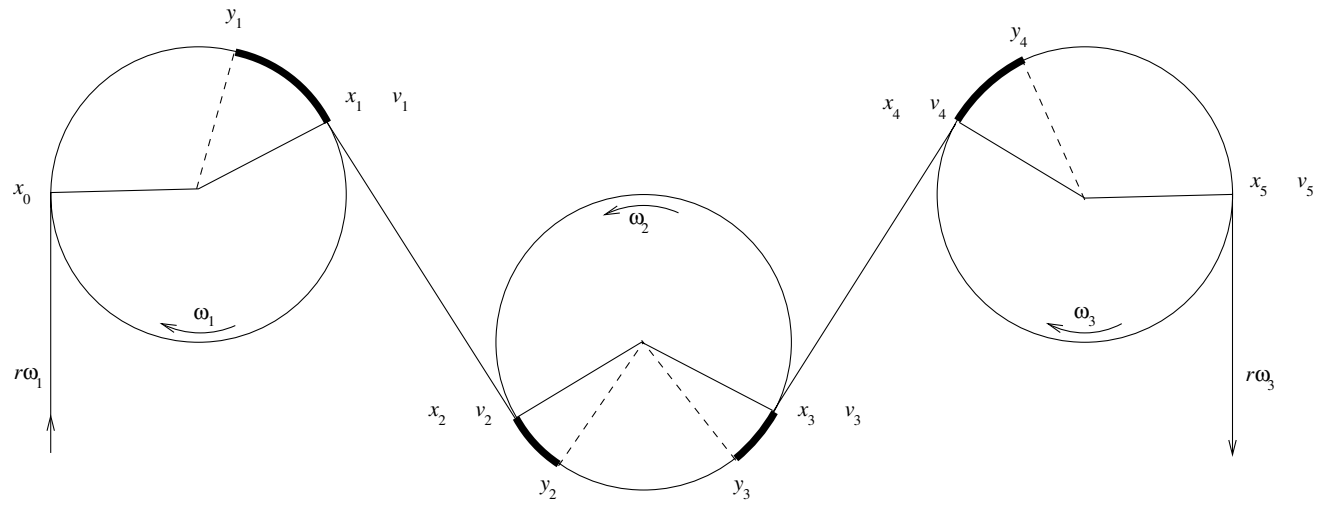

Fig. 1. The possible draw zones for the two-stage process: (1) on the feed roller of the first stage (between y_1 and x_1), (2) in the first freespan (between x_1 and x_2), (3) on the take-up roller of the first stage (between x_2 and y_2), (4) on the feed roller of the second stage (between y_3 and x_3), (5) in the second freespan (between x_3 and x_4), and (6) on the take-up roller of the second stage (between x_4 and y_4).

on surface properties. Gohil and Salem [6] studied the effect of bi-axial drawing of PET film on amorphous (non-crystalline) orientation. They investigated the effect of sequential drawing on producing a "balanced" bi-axial orientation to enhance strength in both directions.

A wide variety of drawing processes are used in industry. The main reason for differences in drawing processes is based on whether the product is a continuous filament yarn or a staple tow (where filaments will be cut to short fiber segments at a later stage). In drawing, filament yarn consists of fewer filaments than staple, which contains thousands of filaments in a yarn or tow. As a consequence, PET filament yarn is generally drawn with radiant heating of the freespan between the rollers. The rollers are not heated, and the draw occurs in the freespan. Staple PET tow is heated using a hot water bath during drawing. As the rollers are also enclosed in the chamber, they are also heated. Owing to the large number of filaments present in a staple tow, a set of feed rollers and a set of take-up rollers are used in the drawing process. Each set of rollers is moving with the same angular velocity, and the draw is achieved by rotating the second set of rollers faster than the first set.

In some processes all the draw is introduced in one step, in a single stage of feed and take-up rollers. This single-stage draw can result in fiber breakage; hence, a two-stage draw is sometimes used in the manufacturing process. In the two-stage process most of the draw (generally between 2.2 and 2.7 draw ratio) is induced in the first step and a relatively smaller draw (1.1–1.2) is applied in the second stage to improve filament strength. One could use multiple draw steps beyond two to introduce draw. The optimal number of stages in the draw is generally determined from extensive experimental effort. As the number of stages is increased, it is possible to keep each freespan and roller at a different temperature and induce the maximum possible draw in each stage in order to obtain the maximum molecular orientation in the fiber. This is the idea behind the new Incremental Draw Process (IDP) [7], in which draw is induced progressively in the fiber using a large number of incremental stages.

What is lacking in the literature is a comprehensive treatment modeling the thermo-mechanical response of fibers under different combinations of thermal histories and windup speeds, which we provide here. In this work we present the fundamental theoretical basis to analyze draw on rollers and in the freespans between rollers, and assemble this knowledge to produce a model for a two-stage industrial draw process. The restriction to two stages is for specificity only; models for drawlines with more than two stages can be constructed in a straightforward manner following the procedure we demonstrate here for two stages. In Section 2 we give a brief description of the draw process, and in Section 3 we establish governing equations for fiber behavior on rollers and in freespans. In Section 4 we assemble solutions to these equations to produce the two-stage draw model, and numerically simulate three processes, i.e. isothermal draw, draw with a heated freespan, and draw with a heated roller.

2. The two-stage draw process

During a two-stage draw process the fiber tow passes over three rollers. We model a two-stage draw process with no guides; see Fig. 1. For simplicity in this paper we take all three rollers to have the same radius r, although this restriction is unnecessary. These rollers rotate at specified constant angular velocities ω_1, ω_2, and ω_3, respectively, each faster than the one before ($\omega_1 < \omega_2 < \omega_3$). Roller 1 functions as the feed roller of the first draw stage; roller 2 functions as both the take-up roller of the first draw stage and the feed

roller of the second draw stage; roller 3 functions as the take-up roller of the second draw stage.

We describe the path of the fibers with space-fixed (Eulerian) arclength s. In our notation, x indicates a specified location, and y and v indicate an unknown location and speed, respectively. As shown in Fig. 1, the fibers attach to the first roller at specified location $s = x_0$ with speed $r\omega_1$ matching the surface speed of the roller. The fibers detach from the first roller at specified location $s = x_1$ with a speed v_1 that will be deduced by the model; v_1 is in general greater than or equal to the roller surface speed $r\omega_1$, indicating the possibility of a draw (i.e. slip) zone on the first roller, in which the fibers are moving faster than the underlying roller surface. The model will also predict the location on the first roller where this draw begins, denoted by y_1. Note we must have $y_1 \leq x_1$: If the model predicts solutions $y_1 < x_1$ and $v_1 > r\omega_1$ then there is draw on the first roller; the region $x_0 \leq s \leq y_1$ is the no-slip zone, and $y_1 < s \leq x_1$ is the draw zone. If the model predicts $y_1 = x_1$ and $v_1 = r\omega_1$ there is no draw on roller 1, i.e. there is no draw on the feed roller of the first stage.

The first freespan extends in our notation from $s = x_1$ to $s = x_2$, where $s = x_2$ is the specified point of attachment to the second roller. The speed v_2 at which the fibers attach to the second roller, to be deduced by the model, is in general greater than or equal to the speed v_1 with which they depart the first roller, so that there is possibly draw in the first freespan. If the model predicts $v_2 > v_1$, then there is draw in the freespan; if $v_2 = v_1$, there is no draw.

Further, the speed v_2 of attachment to the second roller deduced by the model is in general less than or equal to the roller speed $r\omega_2$, so that there is also the possibility of a draw zone on the second roller, where the fiber is moving slower than the underlying roller. The draw on the roller terminates at a location $s = y_2$ to be deduced by the model. In this draw zone $x_2 \leq s < y_2$ the second roller is functioning as the take-up roller of the first stage. If the model predicts $y_2 = x_2$ and $v_2 = r\omega_2$ then there is no take-up draw on roller 2.

Moving down the drawline, the fibers detach from the second roller at a specified location $s = x_3$ with a speed v_3 deduced by the model that is in general greater than or equal to the roller speed $r\omega_2$. Hence the fibers move without slip at roller speed $r\omega_2$ from $s = y_2$ (where the first stage draw ceases) to some point $s = y_3$ where a possible second draw zone on the middle roller begins. In this second draw zone $y_3 < s \leq x_3$ the second roller is functioning as the feed roller of the second stage, and the fibers are moving faster than the underlying roller. Again, a solution $y_3 = x_3$ and $v_3 = r\omega_2$ would indicate that there is no feed draw on roller 2.

The second freespan extends from the location $s = x_3$ of departure from second roller to the location $s = x_4$ of attachment to the third and final roller. The fibers attach to the final roller with a speed v_4 deduced by the model, which in general is greater than or equal to the speed v_3 with which they depart the second roller, so that draw is possible in the second freespan.

The speed v_4 of attachment to the third roller deduced by the model is also in general less than or equal to its surface speed $r\omega_3$, creating the possibility of a take-up draw zone in which the speed of the fibers is less than the underlying roller speed. The slip terminates at $s = y_4$, at which point the fibers have reached the speed $r\omega_3$ of the roller. The fibers maintain this speed until they exit the final roller at $s = x_5$.

Summarizing, in the two-stage draw process without guides draw is possible in six zones, depending on process conditions and the response of the as-spun fiber (see Fig. 1):

1. on the feed roller of the first stage, if $v_1 > r\omega_1$ and $y_1 < x_1$;
2. in the freespan of the first stage, if $v_2 > v_1$;
3. on the take-up roller of the first stage, if $v_2 < r\omega_2$ and $y_2 > x_2$;
4. on the feed roller of the second stage, if $v_3 > r\omega_2$ and $y_3 < x_3$; (note that roller 2 is both the take-up roller for the first draw stage and the feed roller of the second stage);
5. in the freespan of the second stage, if $v_4 > v_3$; and
6. on the take-up roller of the second stage, if $v_4 < r\omega_3$ and $y_4 > x_4$.

For each of these six possible places, draw does not occur if the corresponding inequality above is instead an equality, e.g. there is no draw on the take-up roller of the second stage if $v_4 = r\omega_3$ and $y_4 = x_4$. In the modeling of the two-stage draw, x_1, x_2, x_3, x_4, $r\omega_1$, $r\omega_2$, and $r\omega_3$ are specified, and y_1, y_2, y_3, y_4, v_1, v_2, v_3, and v_4 are deduced.

3. Basic equations and solutions

In this paper we present a theoretical framework to predict the thermo-mechanical behavior of the fibers during drawing that is independent of the particular quantitative constitutive behavior of the fiber. The framework is developed by satisfying the necessary conditions in continuum mechanics (i.e. conservation of mass and momentum). The behavior of the fiber under uniaxial tension for various temperatures must be input, to be obtained ultimately for a particular fiber from measurements of the response of that fiber in uniaxial tension tests. For the demonstration of this paper we use a fiber model of a form which idealizes the typical behavior of undrawn PET fiber, rather than address a particular fiber.

We extend the equations derived in Refs. [9,10] to account for spatial variation in temperature. Recall that we have adopted an Eulerian formulation with the location s fixed in space. We assume the draw process is steady, so that the conditions at location s are independent of time.

Conservation of mass. The mass per unit volume and cross-sectional area of the fibers are denoted by ρ and A,

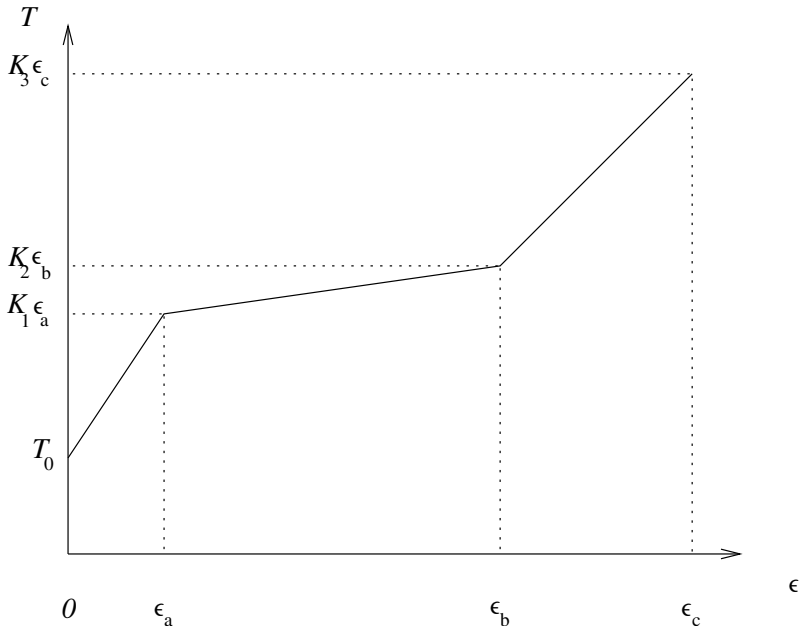

Fig. 2. Constitutive relation between axial force T and strain ϵ in the fiber tow at fixed temperature, valid for processes in which tension and strain increase monotonically down the drawline.

respectively. For this steady motion, conservation of mass requires that the mass flow rate G is constant,

$$G = \rho A(s)v(s) = \text{constant}. \tag{1}$$

Conservation of momentum in a freespan. In Ref. [9] we show that conservation of momentum in a freespan demands that an increment of fiber tension is related to an increment of fiber speed through

$$\mathrm{d}T = G\,\mathrm{d}v. \tag{2}$$

Conservation of momentum on a roller. We denote by f and n the projections of the force per unit length from the roller on the fibers in the tangential and normal directions, respectively, and assign positive n to be compressive and positive f to be in the direction of decreasing s. Where there is no slip, the sign and magnitude of friction depends on the demands of the momentum equation. Where there is slip we assume that the magnitude of f is given by

$$|f| = \mu(\Theta)n, \tag{3}$$

where for specificity the coefficient of friction is a function of temperature Θ (as in Ref. [8], μ could also be considered as a function of filament speed v, resulting in only minor changes to the following analysis). According to our sign convention on friction, f is positive if the fibers are moving faster than the roller surface (as in draw on a feed roller) and negative if the fibers are moving slower (as in draw on a take-up roller). We ignore aerodynamic forces and viscous heating, and conservation of momentum projected in the tangential and normal directions are

$$\mathrm{d}T - f\,\mathrm{d}s = G\,\mathrm{d}v, \qquad n = \frac{T - Gv}{r}. \tag{4}$$

Solutions to the draw model must satisfy the condition that the normal force per unit length n from the roller on the fibers be compressive or zero (non-negative according to our sign convention), which, combined with the second of Eq. (4), demands

$$T - Gv \geq 0. \tag{5}$$

Constitutive behavior. We assume that in the draw process the fibers of the tow form a layer resembling a belt, and every fiber experiences equal tension and stretch. We characterize the fiber tow as thermoelastic–plastic, i.e. the increment $\mathrm{d}T$ of tensile force in a fiber at a point depends on the tow's axial strain ϵ, strain increment $\mathrm{d}\epsilon$, and temperature Θ at that point. We have not included viscous effects in our idealized constitutive model for fiber response during drawing. Viscous effects are highly dependent on the processing temperature, and the draw temperatures we simulate in Section 5 are below the range where viscous effects are important. Moreover, the draw processes we simulate are relatively fast and short (greater than 400 cm/s in drawing spans of about 450 cm), so that the residence times in the draw processes are short. Hence during these processes viscous effects are likely insignificant (although there may be significant relaxation *after* the draw).

The axial strain ϵ at a point s of the tow is

$$\epsilon(s) = \frac{\mathrm{d}l(s)}{\mathrm{d}l_{\mathrm{ref}}} - 1, \tag{6}$$

with $dl(s)$ the length of an infinitesimal section of the fiber at location s and dl_{ref} the length of that section in some reference state. Without loss of generality we select the state of the fiber tow as it attaches to the first roller as the reference state, i.e. the state to which we assign zero strain. The tensile force in the tow as it attaches to the first roller is labeled T_0. In the draw process T_0 is controlled. From constraint (5), this upline tension T_0 must be greater than $Gr\omega_1$; an insufficiently tensioned tow will fly off the roller.

We produce a thermoelastic–plastic constitutive equation for the fiber tow which models the behavior of a soft draw plateau between stiffer regions. This response is typical of as-spun, undrawn polymeric fibers. For small strains the tow is stiff and elastic, with large modulus K_1. When the loading and strain are monotonically increasing throughout the draw line, at a threshold value ϵ_a of strain the modulus abruptly softens to a value K_2 less than K_1, and beyond a second transition strain ϵ_b the modulus again stiffens to a value K_3 greater than the plateau K_2. At strain ϵ_c the filament breaks. See Fig. 2. The moduli K_1, K_2, and K_3 and the strains ϵ_a, ϵ_b, and ϵ_c are specified functions of temperature Θ. In equations, for monotonically increasing loading (i.e. when $d\epsilon \geq 0$ for all s) and uniform temperature,

$$dT = \begin{cases} K_1\, d\epsilon & \text{if } \epsilon \leq \epsilon_a \\ K_2\, d\epsilon & \text{if } \epsilon_a \leq \epsilon \leq \epsilon_b \\ K_3\, d\epsilon & \text{if } \epsilon_b \leq \epsilon \leq \epsilon_c. \end{cases} \tag{7}$$

If the filament unloads, i.e. if $d\epsilon < 0$ at some location s, then $dT = K_1\, d\epsilon$. Therefore if the filament has been loaded beyond the first transition ϵ_a, there is permanent deformation, since $K_2 < K_1$.

In our simulations to follow, we adopt linear dependence of the moduli and transition strains on temperature:

$$\begin{aligned} K_1(\Theta) &= k_{11} + k_{12}(\Theta - \Theta_0), \\ K_2(\Theta) &= k_{21} + k_{22}(\Theta - \Theta_0), \\ K_3(\Theta) &= k_{31} + k_{32}(\Theta - \Theta_0), \end{aligned} \tag{8}$$

(unless the value of temperature is such that the function is negative, in which case the modulus is zero), and

$$\begin{aligned} \epsilon_a(\Theta) &= \epsilon_{11} + \epsilon_{12}(\Theta - \Theta_0), \\ \epsilon_b(\Theta) &= \epsilon_{21} + \epsilon_{22}(\Theta - \Theta_0), \\ \epsilon_c(\Theta) &= \epsilon_{31} + \epsilon_{32}(\Theta - \Theta_0). \end{aligned} \tag{9}$$

In Eqs. (8) and (9), Θ_0 is the temperature of the fibers as they attach to the first roller.

Because there are no guides in the processes we model in this paper, there is no unloading: the increments dT and $d\epsilon$ of fiber tension and strain are positive everywhere, i.e. T and ϵ monotonically increase down the drawline. For such processes, our incremental thermoelastic–plastic constitutive model (7) can be integrated to produce a stress–strain relation for the thermoelastic–plastic fiber, giving tension as a function of strain and temperature,

$$\tilde{T}(\epsilon, \Theta) = \begin{cases} T_0 + K_1\epsilon & \text{if } 0 \leq \epsilon \leq \epsilon_a \\ T_0 + K_1\epsilon_a + K_2(\epsilon - \epsilon_a) & \text{if } \epsilon_a \leq \epsilon \leq \epsilon_b \\ T_0 + K_1\epsilon_a + K_2(\epsilon_b - \epsilon_a) + K_3(\epsilon - \epsilon_b) & \\ \qquad \text{if } \epsilon_b \leq \epsilon \leq \epsilon_c. & \end{cases} \tag{10}$$

This is a special case of the result in plasticity that in uniaxial tension with no unloading (or, most generally, 3D loading in which the stress components monotonically increase during the experiment in proportion to one another, called 'simple,' 'radial,' or 'proportional' loading) the incremental theory relating increment of strain, strain, and increment of stress integrates to a function relating stress to strain, i.e. the equations behave as equations of non-linear elasticity, even though there is permanent deformation [11,12].

For a moving fiber, the strain $\epsilon(s)$ at any point s is related to the fiber speed $v(s)$ at that point and the speed $r\omega_1$ of the fiber in the reference state where it attaches to the first roller by

$$\epsilon(s) = \frac{v(s)}{r\omega_1} - 1. \tag{11}$$

Hence, the constitutive equation (10) can be recast as tension as a function of fiber speed and temperature,

$$\tilde{T}(v, \Theta) = \begin{cases} T_0 + K_1\left(\dfrac{v}{r\omega_1} - 1\right) & \text{if } r\omega_1 \leq v \leq v_a \\ T_0 + K_1\left(\dfrac{v_a}{r\omega_1} - 1\right) + K_2\left(\dfrac{v}{r\omega_1} - \dfrac{v_a}{r\omega_1}\right) & \\ \qquad \text{if } v_a \leq v \leq v_b & \\ T_0 + K_1\left(\dfrac{v_a}{r\omega_1} - 1\right) + K_2\left(\dfrac{v_b}{r\omega_1} - \dfrac{v_a}{r\omega_1}\right) & \\ +K_3\left(\dfrac{v}{r\omega_1} - \dfrac{v_b}{r\omega_1}\right) & \\ \qquad \text{if } v_b \leq v \leq v_c, & \end{cases} \tag{12}$$

where $v_a = r\omega_1(1 + \epsilon_a)$, $v_b = r\omega_1(1 + \epsilon_b)$, and $v_c = r\omega_1(1 + \epsilon_c)$ are specified functions deduced from Eq. (9). From Eqs. (8) and (12) we have that an increment of force dT is related to increments dv and $d\Theta$ of speed and temperature, respectively, through

$$dT = \frac{\partial \tilde{T}}{\partial v}\, dv + \frac{\partial \tilde{T}}{\partial \Theta}\, d\Theta, \tag{13}$$

Table 1
Values of material constants of Eqs. (8) and (9) used in the simulations to characterize the fiber tow

Constant	Value	Units
T_0	40000	dyn
k_{11}	39043800	dyn
k_{12}	−98100	dyn K^{-1}
k_{21}	29459	dyn
k_{22}	0.1962	dyn K^{-1}
k_{31}	882900	dyn
k_{32}	1962	dyn K^{-1}
ϵ_{11}	0.025	
ϵ_{12}	−0.00025	K^{-1}
ϵ_{21}	0.70	
ϵ_{22}	0.0002	K^{-1}
ϵ_{31}	2.3219	
ϵ_{32}	0.0003	K^{-1}

where

$$\frac{\partial \tilde{T}}{\partial v} = \begin{cases} \frac{1}{r\omega_1}(k_{11} + k_{12}(\Theta - \Theta_0)) & \text{if } v \le v_a \\ \frac{1}{r\omega_1}(k_{21} + k_{22}(\Theta - \Theta_0)) & \text{if } v_a \le v \le v_b \\ \frac{1}{r\omega_1}(k_{31} + k_{32}(\Theta - \Theta_0)) & \text{if } v_b \le v \le v_c, \end{cases}$$

and

$$\frac{\partial \tilde{T}}{\partial \Theta} = \begin{cases} k_{12}\left(\frac{v}{r\omega_1} - 1\right) & \text{if } v \le v_a \\ k_{12}\left(\frac{v_a}{r\omega_1} - 1\right) + k_{22}\left(\frac{v}{r\omega_1} - \frac{v_a}{r\omega_1}\right) & \text{if } v_a \le v \le v_b \\ k_{12}\left(\frac{v_a}{r\omega_1} - 1\right) + k_{22}\left(\frac{v_b}{r\omega_1} - \frac{v_a}{r\omega_1}\right) & \\ +k_{32}\left(\frac{v}{r\omega_1} - \frac{v_b}{r\omega_1}\right) & \text{if } v_b \le v \le v_c. \end{cases}$$

The values of material constants used in the simulations to follow are in Table l. For the signs of k_{11}, k_{12}, k_{21}, k_{22}, k_{31}, k_{32}, ϵ_{11}, ϵ_{12}, ϵ_{21}, ϵ_{22}, ϵ_{31}, and ϵ_{32} given in Table 1, the stiffness K_1 of the initial elastic zone decreases, and the stiffnesses K_2 and K_3 of the subsequent zones and width of the compliant intermediate draw plateau increase, with increasing temperature. (Typically, the initial elastic stiffness K_1 of an undrawn fiber decreases with increasing temperature [13]. Beyond the elastic range the stiffness of the fibers is strongly influenced by the amorphous orientation and the degree of crystallinity induced by the draw, and the relative proportion of extended chain crystals vs. folded chain crystals present in the fiber, which in turn

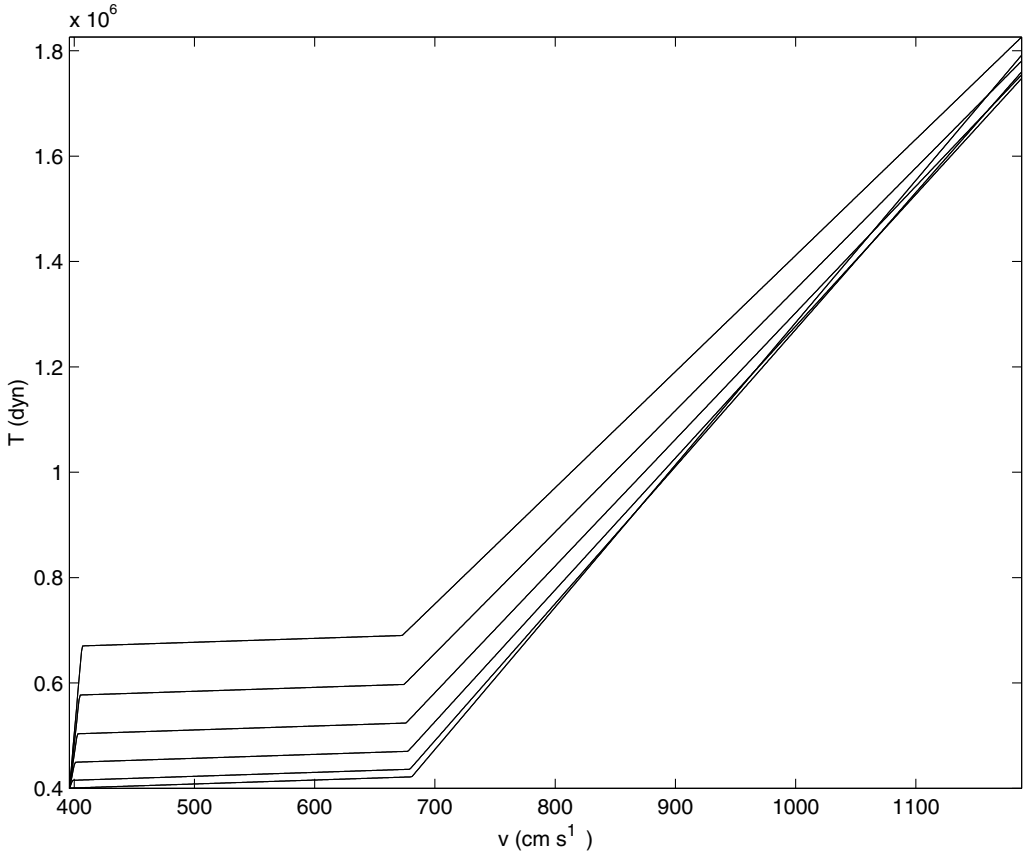

Fig. 3. Constitutive relation between axial force and speed employed in the simulations as temperature increases from 293 to 323 K (top to bottom) in increments of 20 K.

are influenced by temperature. Hence, morphological changes in the fiber could explain the experimental observations that a higher stiffness is observed for the third stage (i.e. the stiff stage after the draw plateau) when the uniaxial tension test is carried out at higher temperatures. Our choices in Table 1 qualitatively account for the temperature dependence of these morphological factors affecting fiber stiffness.) Fig. 3 displays the relation (12) between fiber tension and speed with the values of Table 1 at several temperatures.

Solution technique. In a fully coupled thermo-mechanical problem, the mass, momentum, and constitutive equations of this section are combined with the energy equation, and these coupled equations are solved simultaneously for the fiber speed $v(s)$, tension $T(s)$, and temperature $\Theta(s)$. An alternative to solving for temperature from the coupled problem is to measure it on-line; with $\Theta(s)$ known, the mechanical equations decouple. This latter approach is followed here: we specify $\Theta(s)$, and solve the mass, momentum, and constitutive equations for $v(s)$ and $T(s)$.

In the draw process the fibers are either in a freespan or on a roller; on a roller the possible conditions are no-slip, draw on a feed roller (i.e. slip with the fibers moving faster than the roller surface), and draw on a take-up roller (i.e. slip with the fibers moving slower than the roller surface). We now integrate the combined momentum, friction, and constitutive equations in each of these cases to obtain closed form solutions for fiber speed and tension.

3.1. Freespan

In the freespan the relevant equations are Eqs. (1), (2), and (13). Combining these results in

$$\frac{\mathrm{d}v}{\mathrm{d}s} = \frac{(\partial\tilde{T}/\partial\Theta)(\mathrm{d}\Theta/\mathrm{d}s)}{G - (\partial\tilde{T}/\partial v)}, \tag{14}$$

where $\partial\tilde{T}/\partial\Theta$ and $\partial\tilde{T}/\partial v$ are given explicitly in Eq. (13). Referring to Fig. 1, in the two-stage process Eq. (14) is valid in the freespans $x_1 < s < x_2$ and $x_3 < s < x_4$. We integrate Eq. (14) from the beginning to end of each freespan:

$$\begin{aligned} v_2 &= v_1 + \int_{x_1}^{x_2} \frac{(\partial\tilde{T}/\partial\Theta)(\mathrm{d}\Theta/\mathrm{d}s)}{G - (\partial\tilde{T}/\partial v)}\,\mathrm{d}s, \\ v_4 &= v_3 + \int_{x_3}^{x_4} \frac{(\partial\tilde{T}/\partial\Theta)(\mathrm{d}\Theta/\mathrm{d}s)}{G - (\partial\tilde{T}/\partial v)}\,\mathrm{d}s. \end{aligned} \tag{15}$$

Eq. (15) involves the four unknowns v_1, v_2, v_3, and v_4; once they are known, the speed as a function of arclength within each freespan is given by

$$v(s) = \begin{cases} v_1 + \displaystyle\int_{x_1}^{s} \frac{(\partial\tilde{T}/\partial\Theta)(\mathrm{d}\Theta/\mathrm{d}s)}{G - (\partial\tilde{T}/\partial v)}\,\mathrm{d}s & \text{if } x_1 < s < x_2, \\ v_3 + \displaystyle\int_{x_3}^{s} \frac{(\partial\tilde{T}/\partial\Theta)(\mathrm{d}\Theta/\mathrm{d}s)}{G - (\partial\tilde{T}/\partial v)}\,\mathrm{d}s & \text{if } x_3 < s < x_4. \end{cases} \tag{16}$$

Inserting this function into the constitutive equation (12) produces fiber tension $T(s)$.

3.2. Draw on a feed roller

When draw occurs on the feed roller, in that slip zone the fiber is moving faster than the roller surface. Friction is kinetic due to the slip, and positive according to our sign convention. Hence Eq. (3) becomes

$$f = \mu n. \tag{17}$$

The relevant equations for draw on a feed roller are thus Eqs. (1), (4), (13), and (17); combining these produces

$$\frac{\mathrm{d}v}{\mathrm{d}s} = \frac{(\partial\tilde{T}/\partial\Theta)(\mathrm{d}\Theta/\mathrm{d}s) - (\mu/r)(T - Gv)}{G - (\partial\tilde{T}/\partial v)}. \tag{18}$$

Referring to Fig. 1, in the two-stage process Eq. (18) is valid in the feed roller draw zones $y_1 < s \le x_1$ and $y_3 < s \le x_3$. We integrate Eq. (18) from point of slip initiation to point departure from the roller for each feed roller draw zone to obtain

$$\begin{aligned} x_1 &= y_1 + \int_{r\omega_1}^{v_1} \frac{G - (\partial\tilde{T}/\partial v)}{(\partial\tilde{T}/\partial\Theta)(\mathrm{d}\Theta/\mathrm{d}s) - (\mu/r)(T - Gv)}\,\mathrm{d}v, \\ x_3 &= y_3 + \int_{r\omega_2}^{v_3} \frac{G - (\partial\tilde{T}/\partial v)}{(\partial\tilde{T}/\partial\Theta)(\mathrm{d}\Theta/\mathrm{d}s) - (\mu/r)(T - Gv)}\,\mathrm{d}v; \end{aligned} \tag{19}$$

the departure speeds v_1 and v_3 deduced by the model must be in the ranges $r\omega_1 \le v_1 \le r\omega_2$ and $r\omega_2 \le v_3 \le r\omega_3$. Solutions y_1 and y_3 of Eq. (19) must satisfy the conditions

$$y_1 \le x_1, \qquad y_3 \le x_3, \tag{20}$$

i.e. the draw zone must be on the roller. If for a particular constitutive relation and temperature profile the first of conditions (20) is not satisfied by the solution of the first equation of Eq. (19), then it is replaced by $y_1 = x_1$; i.e. there is no draw on the feed roller of the first stage. If the solution of the second equation of Eq. (19) does not satisfy the second of conditions (20), then it is replaced by $y_3 = x_3$.

Eq. (19) involves the four unknowns y_1, y_3, v_1, and v_3; once they are known, the fiber speed as a function of s

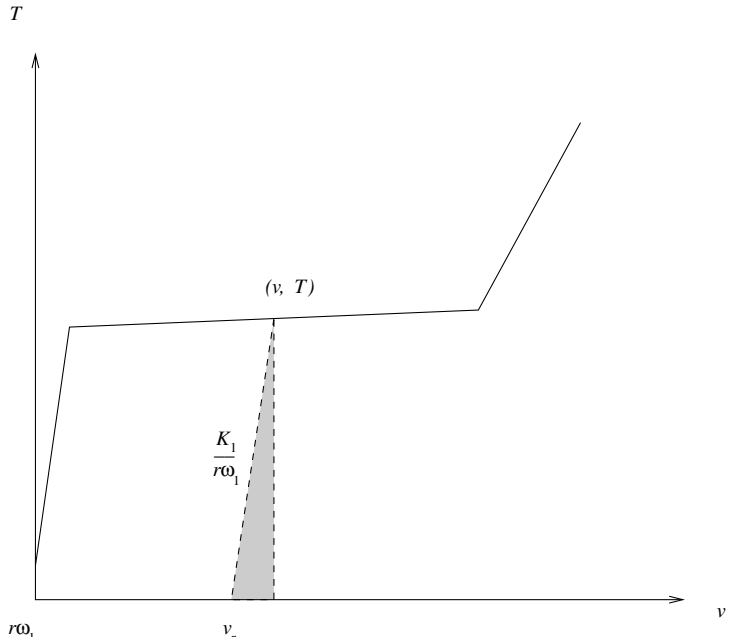

Fig. 4. The shaded area indicates the power that can be recovered from the fiber at speed v and corresponding tension T; vr is the speed of the permanently stretched, unloaded fiber.

within the draw zones is

$$v(s) = \begin{cases} v_1 + \int_{x_1}^{s} \dfrac{(\partial\tilde{T}/\partial\Theta)(\mathrm{d}\Theta/\mathrm{d}s) - (\mu/r)(T - Gv)}{G - (\partial\tilde{T}/\partial v)}\,\mathrm{d}s \\ \qquad \text{if } y_1 < s \le x_1, \\ v_3 + \int_{x_3}^{s} \dfrac{(\partial\tilde{T}/\partial\Theta)(\mathrm{d}\Theta/\mathrm{d}s) - (\mu/r)(T - Gv)}{G - (\partial\tilde{T}/\partial v)}\,\mathrm{d}s \\ \qquad \text{if } y_3 < s \le x_3. \end{cases} \tag{21}$$

Again, inserting this function into the constitutive equation (12) produces fiber tension $T(s)$.

3.3. Draw on a take-up roller

When draw occurs on the take-up roller, in that slip zone the fiber is moving slower than the roller surface. Friction is kinetic due to the slip, and negative according to our sign convention. Hence Eq. (3) becomes

$$f = -\mu n. \tag{22}$$

The relevant equations for draw on a take-up roller are Eqs. (1), (4), (13), and (22); combining these produces

$$\frac{\mathrm{d}v}{\mathrm{d}s} = \frac{(\partial\tilde{T}/\partial\Theta)(\mathrm{d}\Theta/\mathrm{d}s) + (\mu/r)(T - Gv)}{G - (\partial\tilde{T}/\partial v)}. \tag{23}$$

This equation is valid in the take-up roller draw zones $x_2 \le s < y_2$ and $x_4 \le s < y_4$. We integrate Eq. (23) from the point of roller attachment to the point of slip termination,

$$\begin{aligned} y_2 &= x_2 + \int_{v_2}^{r\omega_2} \frac{G - (\partial\tilde{T}/\partial v)}{(\partial\tilde{T}/\partial\Theta)(\mathrm{d}\Theta/\mathrm{d}s) + (\mu/r)(T - Gv)}\,\mathrm{d}v, \\ y_4 &= x_4 + \int_{v_4}^{r\omega_3} \frac{G - (\partial\tilde{T}/\partial v)}{(\partial\tilde{T}/\partial\Theta)(\mathrm{d}\Theta/\mathrm{d}s) + (\mu/r)(T - Gv)}\,\mathrm{d}v; \end{aligned} \tag{24}$$

the attachment speeds v_2 and v_4 deduced by the model must be in the ranges $r\omega_1 \le v_2 \le r\omega_2$ and $r\omega_2 \le v_4 \le r\omega_3$. Solutions of y_2 and y_4 of Eq. (24) must be consistent with the conditions

$$y_2 \ge x_2, \qquad y_4 \ge x_4; \tag{25}$$

otherwise they are replaced by $y_2 = x_2$, and $y_4 = x_4$, respectively.

Eq. (24) involves the four unknowns y_2, y_4, v_2, and v_4; once they are known, the fiber speed as a function of s within the draw zones is

$$v(s) = \begin{cases} v_2 + \int_{x_2}^{s} \dfrac{(\partial\tilde{T}/\partial\Theta)(\mathrm{d}\Theta/\mathrm{d}s) + (\mu/r)(T - Gv)}{G - (\partial\tilde{T}/\partial v)}\,\mathrm{d}s \\ \qquad \text{if } x_2 \le s < y_2, \\ v_4 + \int_{x_4}^{s} \dfrac{(\partial\tilde{T}/\partial\Theta)(\mathrm{d}\Theta/\mathrm{d}s) + (\mu/r)(T - Gv)}{G - (\partial\tilde{T}/\partial v)}\,\mathrm{d}s \\ \qquad \text{if } x_4 \le s < y_4. \end{cases} \tag{26}$$

Fig. 5. Speed (v), tension (T), normal force per length (n), frictional force per length (f), and temperature profiles (Θ) for an isothermal draw process. Crosses (×) denote locations where the fibers either attach to or depart from a roller, and circles (○) denote locations of the initiation or cessation of slip. Solid lines (—) indicate zones of draw on rollers, dashed–dotted lines (- · -) indicate zones of no slip, and dotted lines (· · ·) indicate freespans.

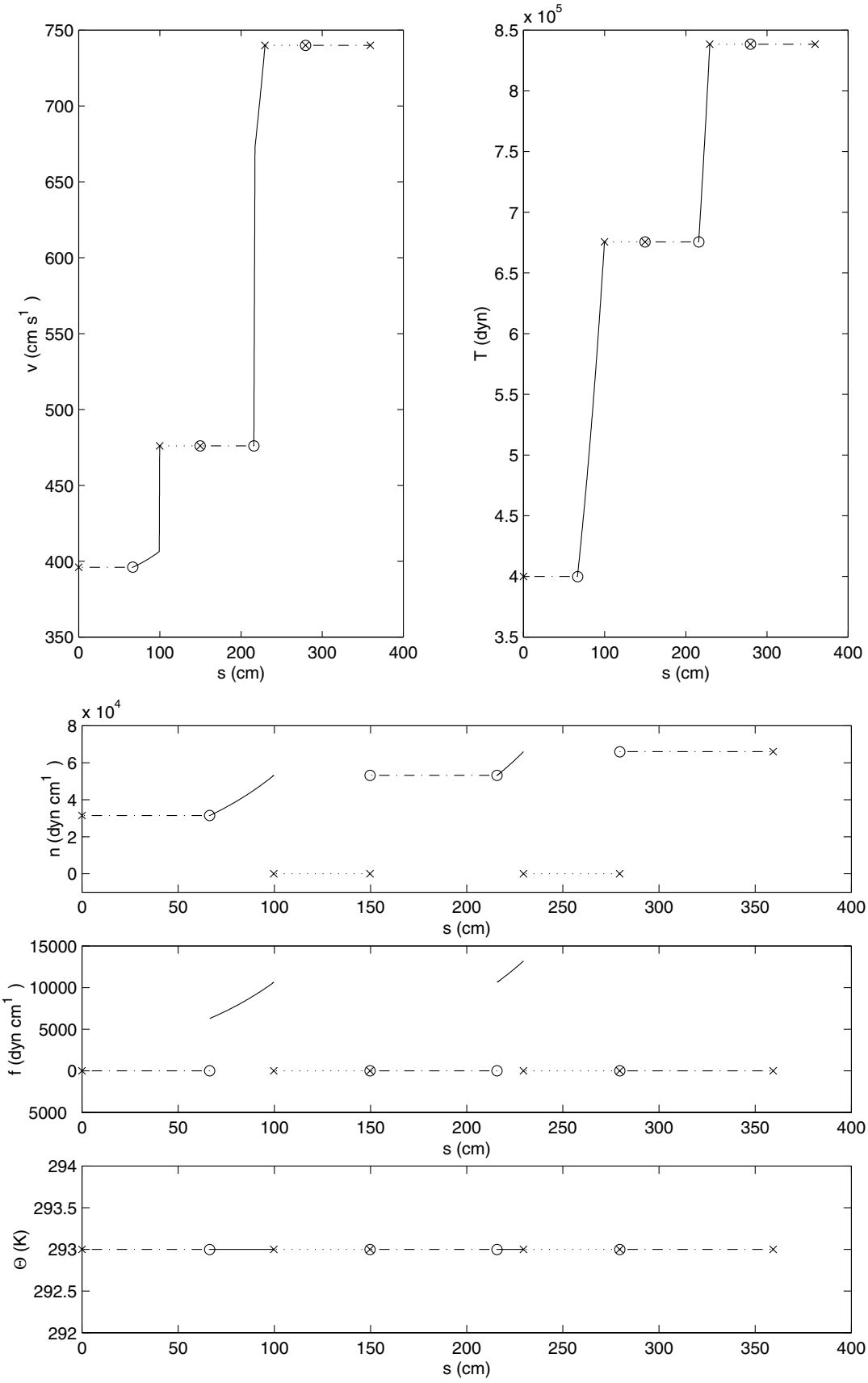
v (cm s^{-1})
s (cm)
T (dyn)
x 10^5
n (dyn cm^{-1})
x 10^4
f (dyn cm^{-1})
Θ (K)

3.4. No-slip on a roller

In the no-slip zones $x_0 \le s \le y_1$, $y_2 \le s \le y_3$, and $y_4 \le s \le x_5$, the fiber speed matches that of the underlying roller surface, and hence is constant. Therefore in these ranges of s,

$$\frac{dv}{ds} = 0. \tag{27}$$

Using Eq. (27), the momentum projection given by the first part of Eq. (4) reduces to an equation for the friction force,

$$f = -\frac{\partial \tilde{T}}{\partial \Theta}\frac{d\Theta}{ds}. \tag{28}$$

4. Complete model for the two-stage draw process

We now assemble the basic solutions of the previous section to construct a model of an entire two-stage draw process. To simulate a particular process, the tow must be characterized with an explicit constitutive equation $T = \tilde{T}(v, \Theta)$, and a temperature profile $\Theta = \Theta(s)$ must be provided.

In our solution procedure we first solve for the four free boundaries y_1, y_2, y_3, and y_4 between slip and no-slip and four transition speeds v_1, v_2, v_3, and v_4, labeled in Fig. 1. Eqs. (15), (19), and (24) are six equations for the eight unknowns y_1, y_2, y_3, y_4, v_1, v_2, v_3, and v_4, and hence the problem is underdetermined. The two free parameters in the problem exist because our steady formulation does not distinguish stable steady states from unstable steady states. To select which of the two-parameter family of steady solutions is the solution that will be physically sustained, we must either examine the stability of the steady solutions in the context of the time-dependent equations, or appeal to energy considerations. The latter approach is followed here.

We identify v_2 and v_4 as the free parameters, noting that they must satisfy $r\omega_1 \le v_2 \le r\omega_2$ and $r\omega_2 \le v_4 \le r\omega_3$, and solve Eqs. (15), (19), and (24) for y_1, y_2, y_3, y_4, v_1, and v_3 in terms of v_2 and v_4.

With y_1, y_2, y_3, y_4, v_1, and v_3 all known in terms of the free parameters v_2 and v_4, Eqs. (11), (15) and (19) are solved individually for $v(s)$ within each slip zone and freespan. The assembled solution along the drawline is labeled by

$$v = \bar{v}(s; v_2, v_4), \tag{29}$$

where we have denoted its dependence on the free parameters v_2 and v_4. With $v(s)$ computed, we obtain the tensile force,

$$T = \bar{T}(s; v_2, v_4), \tag{30}$$

as a function of position everywhere in the drawline by inserting $v(s; v_2, v_4)$, together with the posited temperature profile $\Theta(s)$, into the constitutive equation (12). The normal and frictional components $\bar{n}(s; v_2, v_4)$ and $\bar{f}(s; v_2, v_4)$ are also obtained from the momentum equations of the previous section once $\bar{v}(s; v_2, v_4)$ has been computed. A different set of solutions v, T, f, and n are produced by each pair of free parameters v_2 and v_4. The stable set is selected as the one corresponding to minimum energy.

Minimization of fiber energy. We propose an energy function which includes kinetic, thermal, and material contributions. The kinetic contribution to this function is $(1/2)Gv^2$, and the thermal contribution is $Gc\Theta$, where c is the specific heat of the fiber material. The material contribution is the recoverable power, shown schematically as the shaded region in Fig. 4. Recall that we assume that the fiber unloads along a line parallel to the first segment of the constitutive relation (12), which has a slope of $K_1/(r\omega_1)$. From Fig. 4 we see that

$$\frac{K_1}{r\omega_1} = \frac{T}{v - v_r}, \qquad \text{or} \qquad v_r = v - \frac{Tr\omega_1}{K_1}. \tag{31}$$

where v_r is the speed of the permanently stretched unloaded fiber. Hence the recoverable power is $(1/2)T(v - v_r) = (1/2)(T^2 r\omega_1)/K_1$. Thus our energy function is constructed from an expression p for power,

$$p = \frac{1}{2}Gv^2 + Gc\Theta + \frac{1}{2}\frac{T^2 r\omega_1}{K_1}. \tag{32}$$

We obtain the energy of the draw line by integrating the power over the residence time of a material particle in the drawline,

$$e = e(v_2, v_4) = \int_{t_0}^{t_f} p\, dt = \int_{x_0}^{x_5} \frac{p}{v}\, ds$$

$$= \int_{x_0}^{x_5} \left(\frac{1}{2}Gv + \frac{Gc\Theta}{v} + \frac{1}{2}\frac{T^2 r\omega_1}{K_1 v} \right) ds. \tag{33}$$

The correct values of the free parameters v_2 and v_4 are those which minimize the energy (Eq. (33)).

5. Simulations

To demonstrate our model, we simulate three different two-stage draw processes. The specification of fiber behavior used in the three simulations, in the context of the constitutive function (12) of Section 3, is given in Table 1.

The first process we simulate is isothermal, the second has a heater in the second freespan, and the third has a heated third roller. These three processes are distinguished by the temperature profile we input. In simulation 1 the temperature is a constant 298 K throughout the process (see Fig. 5); note that in this simulation we neglect passive heating due to internal dissipation from stretching and friction between the fibers and rollers. In simulation 2 the tow temperature is specified to be the same constant 298 K until the second freespan, over which it ramps to 323 K (owing to a freespan heater), then ramps back down to 298 K over the first 5 cm on the unheated third roller (see Fig. 6). In simulation 3 the temperature is a constant 298 K until the fiber

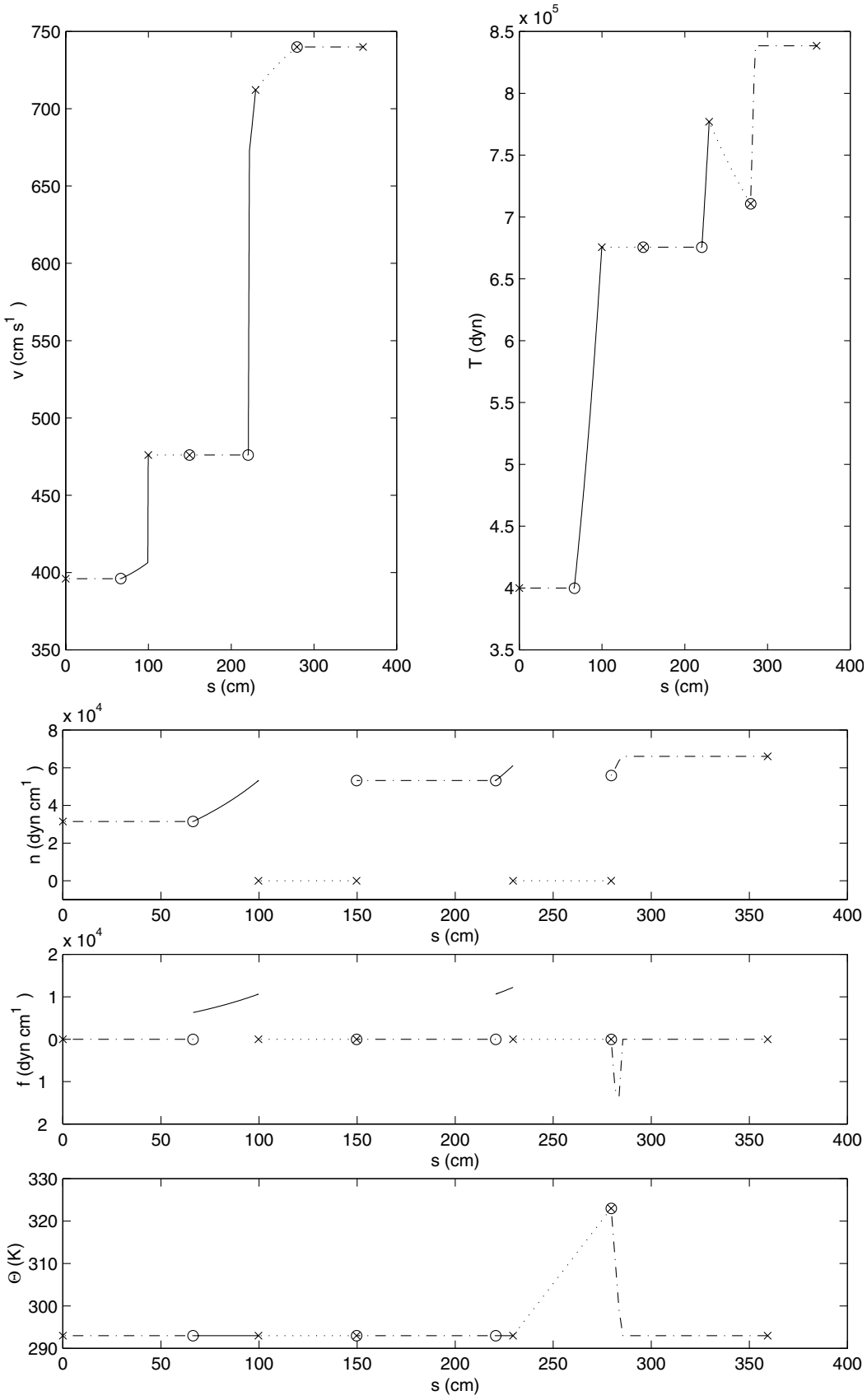

Fig. 6. Speed, tension, normal force per length, frictional force per length, and temperature profiles for a drawline with heated second freespan.

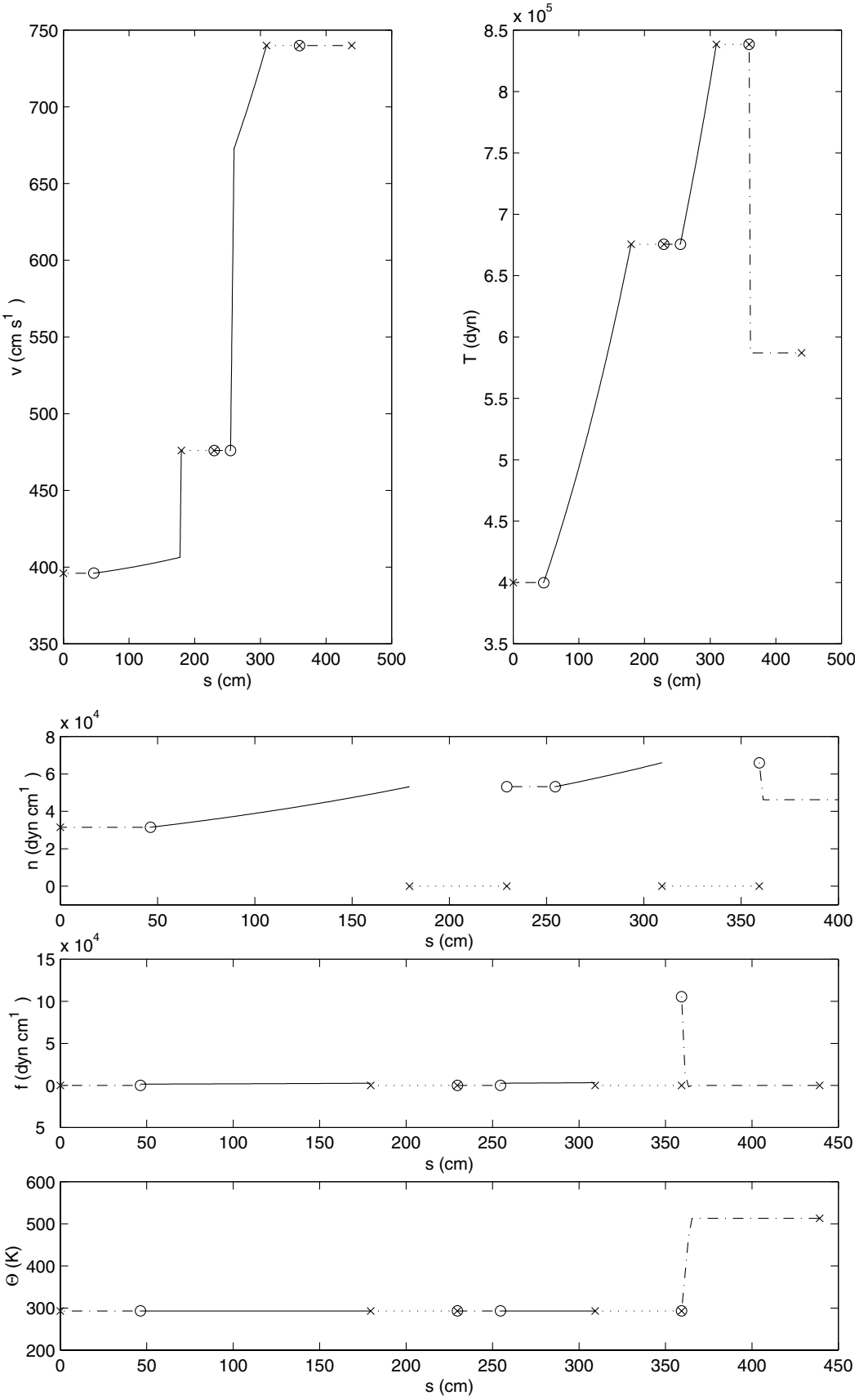

Fig. 7. Speed, tension, normal force per length, frictional force per length, and temperature profiles for a drawline with heated final roller and with $\mu = 0.05$. The drawline length is greater than the previous simulations owing to an added wrap on the first roller.

contacts the heated third roller, then over the first 5 cm of this roller the temperature ramps up to 513 K, thereafter remaining at the roller temperature 513 K (see Fig. 7). The remaining process conditions for the three simulations are displayed in Table 2. Note that, aside from the temperature profiles, the processes of simulations 1 and 2 are identical.

In addition to the temperature profile, simulation 3 differs from the other two in that there is a lower coefficient of friction between the fiber and the rollers ($\mu = 0.05$ rather than 0.2), and there are two and a quarter wraps on the first roller rather than one and a quarter, necessitated by the low friction coefficient. (If there were only one and a quarter wrap in this simulation, the solution of Eq. (19) would yield $y_1 = -33$ cm; the negative value signifies that the necessary draw surface is greater than what is available with just one and a quarter wrap, so the fibers would slip over the entire contact with the roller.)

In each simulation we compute the fiber speed $v(s)$ and tension $T(s)$ throughout the drawline as described in Section 4, and display these functions in the figure above the specified temperature profile. With the computed functions $T(s)$ and $v(s)$, we employ Eq. (4) to deduce the frictional and normal forces per length f and n from the rollers on the fiber as functions of position; these we also display in the figures. In these plots, the superimposed symbols "×" label the locations where the fibers attach to and depart from the rollers (these locations are input to the model), and the symbols "○" label where slip starts in feed draw and ceases in take-up draw (these locations are deduced by the model). The abrupt bends in the speed plot not at a × or ○ indicate the transitions into and out of the draw plateau of the fiber.

Referring to Figs. 5–7, the top left plot displays the computed fiber speed v as a function of arclength s, and the top right plot displays the computed fiber tension $T(s)$.

Table 2
Input for simulation 1 (isothermal draw), simulation 2 (draw with a heated second freespan), and simulation 3 (draw with a heated third roller). The posited temperature profiles are displayed in Figs. 5–7, respectively

Input	Sim. 1	Sim. 2	Sim. 3
Reference temperature, Θ_0 (K)	298	298	298
Coefficient of friction, μ	0.2	0.2	0.05
Linear density of fiber, ρ (denier)	450	450	450
Length of freespan 1 (cm)	50	50	50
Length of freespan 2 (cm)	50	50	50
Roller radius, r (cm)	12.7	12.7	12.7
Number of wraps on roller 1	1.25	1.25	1.25
Number of wraps on roller 2	1	1	1
Number of wraps on roller 3	1	1	1
Roller 1 surface speed, $r\omega_1$ (cm s^{-1})	396	396	396
Roller 2 surface speed, $r\omega_2$ (cm s^{-1})	476	476	476
Roller 3 surface speed $r\omega_3$ (cm s^{-1})	740	740	740

Below this pair in order are the computed normal force per length $n(s)$ from the roller on the fiber, computed frictional force per length $f(s)$ from the roller on the fiber, and specified temperature profile $\Theta(s)$. Proceeding from left to right in each plot, the first × (and beginning of the plot) is the point of attachment $x_0 = 0$ cm of the fiber to roller 1, the second × is the point of departure x_1 from roller 1, the third × is the point of attachment x_2 to roller 2, the fourth × is the point of departure x_3 from roller 2, the fifth × is the point of attachment to the third roller, and the sixth × (and termination of plot) is the point of detachment from the roller 3. The first ○ is the point of initiation y_1 of feed slip on roller 1, the second ○ is the point of cessation y_2 of take-up slip on roller 2, the third ○ is the point of initiation y_3 of feed slip on roller 2, and the fourth ○ is the point of cessation y_4 of take-up slip on roller 3.

In the isothermal simulation (Fig. 5) we find that conditions (25) are violated by the solutions of Eq. (24) for all allowable speeds v_2 and v_4 of attachment with the take-up rollers, $r\omega_1 \le v_2 < r\omega_2$ and $r\omega_2 \le v_4 < r\omega_3$. Hence for the given fiber response function and process conditions draw does not occur on either take-up roller, i.e. the model demands $y_2 = x_2, y_4 = x_4$. Also, since the fiber is isothermal in both freespans ($d\Theta/ds = 0$) and there are no intervening guides, Eq. (14) dictates that speed is constant in both freespans. Therefore, in the isothermal process of simulation 1, of the six possible places of draw listed at the end of Section 2 and in Fig. 1, draw occurs only in the first and fourth, i.e. on the two feed rollers. This is due to our specific process conditions and filament constitutive response.

Referring to Fig. 5, the fiber attaches to roller 1 at the first × ($s = 0$ cm) with tension $T_0 = 4.00 \times 10^5$ dyn and at the surface speed $r\omega_1 = 396$ cm s^{-1}. The fibers proceed without slip on roller 1 until the first ○ at $s = 67$ cm; in this 67 cm of no slip the speed, tension, and normal force per length are all constant, and the friction force per length f is zero ($d\Theta/ds = 0$ implies $f = 0$ in Eq. (28)). The draw zone on roller 1 is the 33 cm from the first ○ ($y_1 = 67$ cm) to the second × ($x_1 = 100$ cm), where the fibers depart the roller. In this draw zone the fiber speed increases from the surface speed 396 cm s^{-1} of roller 1 to the surface speed 476 cm s^{-1} of roller 2, and the tension increases from 4.00×10^5 to 6.76×10^5 dyn. Note from the presence of the kink at $s = 99$ cm in the $v(s)$ plot that the fiber is drawn on the first feed roller from its initial stiff response into its soft plateau. For $67 < s < 99$ cm the draw is in the stiff portion of the filament response, where a large increase in tension accompanies a small increase in strain and hence speed. For $99 < s < 100$ cm the draw is in the soft portion of the filament response, where a small increase in tension accompanies a large increase in strain and speed. In the draw zone the frictional force on the fiber is increasing and in the direction opposite to fiber motion.

The 50 cm between the second × ($x_1 = 100$ cm) and third × ($x_2 = 150$ cm) is the first freespan. In this isothermal freespan without guides, speed and tension are constant.

Note that the second ○ coincides with the third ×, indicating the aforementioned result that there is no take-up draw on roller 2: the fiber attaches to roller 2 at $x_2 = y_2 =$ 150 cm already at its surface speed $r\omega_2 = 476$ cm s^{-1}. The fiber proceeds on roller 2 without slip until the third ○, where it begins to slip; this draw zone on roller 2 is the 14 cm from the third ○ at $y_3 = 216$ cm to the fourth × at $x_3 = 230$ cm, where the fiber departs from roller 2 already at the surface speed of roller 3. Note from the kink in $v(s)$ that the fiber has been drawn out of its soft plateau on the second feed roller.

Between the fourth × and fifth × (at $x_4 = 280$ cm) is the second freespan, again isothermal with no guides and hence without draw. The fourth ○ coincides with the fifth ×, again indicating that there is no take-up draw in this isothermal process. The fiber proceeds without slip on its entire path on roller 3.

Fig. 5 shows that at the location $y_1 = 67$ cm where slip begins, there is a rapid buildup of normal and frictional forces. As the tow stretches, the normal and the frictional forces increase, until they vanish when the tow leaves the roller. The tension in the tow increases uniformly down the drawline. The fiber velocity increases slightly when the extension of the fiber is within the initial stiffer region of the constitutive relation. At $s = 99$ cm, the fiber behavior moves from the first stiff region to the compliant region, and correspondingly the speed of the tow increases rapidly up to the surface speed of roller 2. Between 100 and 216 cm the tow moves through the freespan and the no-slip zone on roller 2 with no changes in the tension and velocity. At $y_3 =$ 216 cm, the tow starts slipping by moving faster than the roller surface, the normal and the frictional forces build up, and the tension increases monotonically. The velocity increases rapidly when the fibers are still in the compliant plateau, but when they enter the second stiffer region the increase in velocity slows down. There are no changes in the tension or velocity in the second freespan, as the process is set up.

In Fig. 6 depicting simulation 2, again note the upward ramp in the temperature profile $\Theta(s)$ between the fourth × and the fifth ×, modeling the heated second freespan, and the downward ramp in $\Theta(s)$ for the first 5 cm after the fifth ×, modeling the cooling of the fibers upon contact with the unheated roller 3. In this process there is draw in *three* of the six possible zones, namely draw on the two feed rollers (as in simulation 1) and also draw in the second freespan because of the presence of the heater. There is no draw in the other three possible zones: the model indicates there is no draw on the two take-up rollers in the same manner as in simulation 1; we find that conditions (25) are violated by solutions of Eq. (24) for all allowable speeds v_2 and v_4. There is no draw in the first freespan since it is isothermal and without guides.

In Fig. 6 the behavior of the tow is identical to that of the isothermal process of simulation 1 until the heated second freespan. When the fibers experience higher temperature, they behave in accordance with the corresponding constitutive equations for that temperature, resulting in reduced tension in the tow as the fibers become softer. Since the fiber can stretch with lower tension in this region, the speed of the fibers increases in this zone in order to match the surface speed of the third roller. The tow enters the third roller without slip, but the decreasing temperature of the fiber induces an increased tension, accompanied by frictional and normal forces, immediately after the tow attaches to the roller.

In our third simulation (Fig. 7), the differences are a lower friction coefficient, two and a quarter wraps on roller 1 (note that the distance between the first × and the second × is now 180 rather than 100 cm), no freespan heaters, and a heated roller 3. For this process there is draw on both feed rollers and no draw on the first (unheated) take-up roller and unheated freespans. Owing to the presence of the heated roller 3, however, there are for the first time in our simulations steady solutions with take-up draw, in which the tow attaches to roller 3 with speed less than the surface speed of roller 3.

When we solve the second equation of Eq. (24), we find solutions of y_4 satisfying $y_4 \geq x_4$ for all values of v_4 between 687.5 and 740 cm s^{-1}. Each of these values produces a steady solution $v(s)$, $T(s)$, $f(s)$, and $n(s)$. Those with $687.5 \leq v_4 < 740$ cm s^{-1} exhibit take-up on the heated roller; that with $v_4 = 740$ cm s^{-1} has no take-up draw. As discussed before, only the steady solution with the lowest energy will be stable and hence persist in the real world. We find that the solution with no take-up draw has the lowest value of the energy function e defined in Eq. (33), and this is the solution exhibited in Fig. 7.

We comment that the reason for the absence of take-up draw on the heated roller 3 is fundamentally different from the reason for no take-up draw on roller 2: on the unheated roller 2 take-up draw is not possible, since the first part of Eq. (24) has no solution satisfying $y_2 > x_2$. On the heated roller 3, take-up draw is possible but unstable.

From Fig. 7 we see that the effect of the heated roller is a large decrease in fiber tension and a large frictional force from the roller when the fiber temperature is increasing. We also note that the lower friction coefficient has produced a much larger draw zone on the first feed roller, and reduced the magnitude of friction. The difference in behavior shown between Figs. 6 and 7 is indicative of the differences in response in filament yarn and staple tow draw processes.

6. Conclusions

A general method of characterizing fiber behavior in a multi-stage draw process is described in this paper. The efficacy of the model is demonstrated for three different two-stage draw processes, with different drawing conditions. The model is flexible to address any fibrous material, as long as its piecewise linear elastic–plastic behavior is

known for a range of temperature conditions. The analysis we present allows one to compare the effectiveness of different drawing conditions, enabling fiber manufacturers to identify optimum processing conditions. The outcome of this analysis is the velocity and tension at any point along the length of the yarn, and the forces from the rollers on the yarn, for specific drawing conditions. These predictions can in turn serve as the input data for investigating micro-structure development in the fiber during drawing. As mentioned earlier, the micro-structure developed in the fiber is responsible for the fiber properties. As the velocity and tension profile is altered, vastly different micro-structure in the fiber could result. The next important step in the study is to couple micro-structure development with the output of this investigation.

Acknowledgements

This work was sponsored in part by the National Textile Center and the US Department of Commerce under Grant E27B51, and the National Science Foundation under Grant CTS-9711109.

References

[1] Botev M, Judeinstein P, Neffati R, Rault J. Macromolecules 1996;29(26):8538–40.
[2] Cansfield DLM, Patel R, Ward IM. J Macromol Sci Phys B 1993;32(4):373–93.
[3] Postema AR, Pennings AJ. J Appl Polym Sci 1989;37(8):2351–69.
[4] Salem DR. Polymer 1994;35(4):771–6.
[5] Hermanutz F, Salem DR, Wesson SP. Polymer 1994;35(21):4611–7.
[6] Gohil RM, Salem DR. J Appl Polym Sci 1993;47(11):1989–98.
[7] Sussman MV. Adv Polym Technol 1993;12(3):291–6.
[8] Amijima S. Sci Engng Rev Doshisha Univ 1962;3(3/4):99–111.
[9] Bechtel SE, Vohra S, Jacob KI, Carlson CD. J Appl Mech 2000;67(1):197–206.
[10] Bechtel SE, Vohra S, Jacob KI. Textile Research Journal (submitted).
[11] Kachanov LM. Fundamentals of the theory of plasticity. Moscow: Mir, 1974.
[12] Lubliner J. Plasticity theory. Macmillan, 1990.
[13] Ziabicki A. Fundamentals of fiber formation. New York: Wiley, 1976.